Inflation and Contact Predictions of Composite Tire Shell Carcass

Sunil Saigal*
Worcester Polytechnic Institute, Worcester, Massachusetts
and
T. Y. Yang† and W. Soedel‡
Purdue University, West Lafayette, Indiana

A passenger car tire is analyzed by treating it as a laminated, anisotropic thin shell that deforms according to the classical Love hypothesis. The tire is modeled using a high-order, doubly curved, quadrilateral thin-shell finite element. The element employs variable-order polynomials for the definition of geometry of the structure and, thus, provides an accurate modeling of the initial profile of the tire, which significantly affects the response of the tire. The material properties of the cord-rubber system forming the tire carcass are assumed as piecewise homogeneous and are obtained by employing the fundamentals of composite material theory. The effect of geometric nonlinearity is included in the formulation to account for stiffening or weakening of the carcass due to deformation. A detailed investigation of deformation and stresses in the tire due to inflation is first made using a load increment algorithm. The inflated tire is next brought into static contact against a rigid surface in a displacement increment procedure to study 1) the displaced profile of the tire in contact, 2) the redistribution of resultant forces and moments in the tire due to contact, 3) the force required to bring the tire in contact, and 4) the footprint of the tire. The developments discussed in this paper may be applied to the study of deformation mechanics in aircraft tires.

Introduction

TWO of the key elements in the analysis of tires are: 1) development of a structural model to represent the deflection characteristics of the tire, and 2) development of a material model to provide the constitutive properties of the tire. Surveys of evolution of such structural and material models may be found in papers by, among others, Patel et al.[1-3] Presently, the finite-element method is a widely accepted technique in the tire structural mechanics. Also, the fundamentals of composite materials technology are commonly used to obtain material properties of the tire, given the measured material constants of tire cords and rubber stock. Various types of finite elements, such as truss and beam elements, two-dimensional plane stress elements, axisymmetric solid elements, and plate elements, have been employed to study the deformation of tires under inflation pressure. A survey of such efforts is given in Refs. 3 and 4. Another aspect of significance in tire design is the knowledge of tire behavior when in contact with a rigid surface. Not many research efforts have been directed in this direction. Deak[5] studied the static contact of a bias tire against a rigid surface using hybrid stress finite elements. The first attempt at obtaining detailed displacements and stresses in a steel-belted radial passenger car tire resulting from contact against a flat surface was made by DeEskinazi[6,7] using the displacement finite-element model. Some limitations of this study were noted as:

1) Triangular flat-plate elements were used to model the geometry of the tire shell resulting in an approximate representation of the geometry of the tire due to faceting of the surface. In addition, structural membrane-bending coupling within an element is not accounted for when flat elements are used. This may result in inaccurate prediction of tire behavior, which is believed to depend significantly on the initial geometry of the tire.

2) The contribution of matrix [*B*], which couples the bending and membrane stresses in the material constitutive relations, was ignored.

3) For the analysis of contact of the tire against a rigid surface, a piecewise linear displacement increment algorithm was used. However, no iterations were performed for these increments so that at the end of each step equilibrium was not assured.

4) A lumping procedure was used in determining the nodal loads corresponding to the inflation pressure.

The present study was aimed at a refined analysis of tire inflation and static contact behavior. A doubly curved, thin-shell finite element including geometric nonlinearity and capable of accurately modeling the initial geometry of the tire was used. Consistent or work-equivalent nodal loads were used, and the effect of the membrane-bending coupling material matrix [*B*] was included. The inflation of the tire was first performed using a load increment algorithm to study the displacement profiles and stresses in the inflated tire. A displacement increment technique was used next to study the contact of the tire against a rigid surface. Iterations were performed for each load or displacement increment to assure equilibrium of the tire. Limitations and scope for further improvement of the present developments will be discussed in this paper.

Doubly Curved, Thin-Shell Finite Element

A doubly curved, thin-shell finite element was used to model the tire. The element has four nodes, one at each corner, and each node has 12 DOF's: $\bar{u}$, $\partial\bar{u}/\partial\xi$, $\partial\bar{u}/\partial\eta$, $\partial^2\bar{u}/\partial\xi\partial\eta$, and similarly for $\bar{v}$ and $\bar{w}$. $\bar{u},\bar{v}$, and $\bar{w}$ are the displacements along the Cartesian directions x,y, and z, respectively, and ξ and η are orthogonal curvilinear coordinates along the shell

Received July 14, 1986; revision received March 13, 1987.

*Assistant Professor, Mechanical Engineering Department. Associate Member AIAA.
†Professor of Aeronautics and Astronautics and Dean of Engineering. Fellow AIAA.
‡Professor, School of Mechanical Engineering.

surface. Bicubic Hermitian polynomials are used to describe the shape functions of the element. The geometry of the shell is modeled using variable-order polynomials. The Cartesian coordinates x^i of the middle surface are expressed as

$$x^i(\xi,\eta) = \sum_{j=1}^{N} c_j^i \xi^{m_j} \eta^{n_j} \tag{1}$$

where the constants m_j and n_j define the powers of ξ and η, respectively, for the jth term. The constants c_j^i are solved based on the coordinates x^i at N selected points on the middle surface of the shell element. Similarly, B-spline and rational B-spline polynomials can also be employed to represent the shell surface geometry. The strain-displacement relations are based on the Love-Kirchhoff thin-shell theory, and the total Lagrangian formulation is adopted for treatment of geometric nonlinearity. The validity of the element has been established through comparisons with existing shell solutions for both isotropic shells[8] and laminated composite shells.[9] References 8 and 9 also provide a detailed explanation of the formulation of the finite element.

Tire Material Model

The tire used in this analysis was a steel-belted radial passenger car tire. The laminate construction of the tire was categorized into six zones along the meridional direction. Each of these zones was considered to possess homogeneous material properties. Assuming that the structural action of the tire is provided mainly by belt plies, the meridional profile of the reference surface of the tire shell was passed through the middle of these plies. The layup of the body plies, the belt ply, and the rubber stock was then determined with respect to this reference surface. For the belt and body ply, the in-plane composite properties are computed using the Halpin-Tsai equations. The stress-strain relations are determined by integrating through the thickness after applying appropriate coordinate transformation for each ply based on the orientation of the ply. Details and a survey of this procedure are given by, among others, Walter et al.[10] The material properties used for the individual plies and rubber stocks were obtained experimentally.

Load and Displacement Increment Procedures

The overall equilibrium equations assembled for the entire system are written in incremental form as

$$\{\Delta P\} = [K_{NL}]\{\Delta Q\} \tag{2}$$

where $\{\Delta P\}$ and $\{\Delta Q\}$ are the vectors of nodal load and displacement increments, respectively, and $[K_{NL}]$ is the assembled stiffness matrix for the entire system, including the contribution due to geometric nonlinearity. The details of derivation of the stiffness matrix can be found in Ref. 8.

Inflation Analysis

A stepwise linear load increment procedure is used for determining tire behavior under inflation pressure. The Newton-Raphson iteration technique is adopted to obtain equilibrium for each load increment step. The details of this procedure are standard and may be found in textbooks, e.g., Ref. 11.

Static Contact Analysis

A stepwise linear displacement increment procedure is employed to simulate the contact of the tire against a rigid surface. The displacement increments for the nodes already in contact or desired to be brought into contact are specified for each step. The total vertical displacement for a step is decided and, starting with the lowest node in the vertical direction, all of the nodes that lie within the total displacement specified are moved upward to the same level. Free movement of these nodes in the horizontal direction is allowed, assuming the rigid surface is frictionless. The displacement increment procedure is a modification of that given in Ref. 6 and is briefly recapitulated subsequently.

The equilibrium equation (2) is partitioned into groups corresponding to the known displacements $\{\Delta Q_K\}$ specified as explained previously and the unknown displacements $\{\Delta Q_u\}$

$$\begin{Bmatrix} \Delta P_u \\ \Delta P_K \end{Bmatrix} = \begin{bmatrix} K_{uu} & K_{uk} \\ K_{ku} & K_{kk} \end{bmatrix} \begin{Bmatrix} \Delta Q_u \\ \Delta Q_k \end{Bmatrix} \tag{3}$$

Since there are no external forces acting at the points that are not in contact, the load vector $\{\Delta P_u\}$ contains only zeros. Substituting $\{\Delta P_u\} = \{0\}$, the first of Eq. (3) yields

$$\{\Delta Q_u\} = -[K_{uu}]^{-1}[K_{uk}]\{\Delta Q_K\} \tag{4}$$

Substituting for $\{\Delta Q_u\}$ from Eq. (4) into the second part of Eq. (3) gives

$$\{\Delta P_k\} = [[K_{kk}] - [K_{ku}][K_{uu}]^{-1}[K_{uk}]]\{\Delta Q_k\} \tag{5}$$

The total load and displacement vectors are updated using these respective increments. Since the stiffness matrix $[K_{NL}]$ is nonlinear and depends on the current displacements, equilibrium of the structure may not be satisfied at this point. An iterative procedure was used to reach the equilibrium state within a specified tolerance. Based on the current displacements, the internal force vector can be obtained as in[8]

$$\{R\} = \int_{\text{vol}} [B^T]\{\sigma\} dV \tag{6}$$

where $\{R\}$ is the vector of internal forces, $[B]$ the strain-displacement matrix, and $\{\sigma\}$ the vector of stresses corresponding to the current displacement state. The unbalance between the externally applied loads and the internal forces is obtained as $\{\psi\} = \{P\} - \{R\}$. The unbalanced load is applied on the structure by replacing $\{\Delta P\}$ in Eq. (2) by $\{\psi\}$ and noting that $\{\Delta Q_K\} = \{0\}$ for equilibrium iterations. Partitioning as in Eq. (3), an additional displacement increment can be obtained as

$$\{\Delta Q_u\} = [K_{uu}]^{-1}\{\Psi_u\} \tag{7}$$

and an additional load increment can be obtained as

$$\{\Delta P_k\} = [K_{ku}]\{\Delta Q_u\} \tag{8}$$

The procedure is repeated until the unbalanced forces $\{\psi\}$ are zero within specified tolerance. Equilibrium was assured for each displacement increment step in the present study to a tolerance of 1%.

Many algorithms for obtaining static contact solutions have been proposed. The shell-of-revolution contact algorithm proposed by Tielking[12] is a method of obtaining a point load influence coefficient matrix for the portion of the shell surface that is expected to carry a contact load. If the shell is sufficiently linear with respect to contact loading, a single influence coefficient matrix can be used to obtain a good approximation of the contact pressure distribution. Otherwise, the matrix is updated to reflect nonlinear load-deflection behavior. The solid body contact algorithm[12] utilizes a Lagrange multiplier to include the contact constraint in a potential energy functional. The solution is found by applying the principle of minimum potential energy. The Lagrange multiplier is identified as the contact load resultant for a specific deflection. The Lagrange multiplier methods satisfy the constraint condition by transforming the constrained problem into an unconstrained one with the introduction of additional variables (Lagrange multipliers). Penalty methods have also been

developed for the contact problem[13,14] and these enable one to transform the constrained problem into an unconstrained one without introducing additional variables. Simo et al.[15] have presented a general overview of these algorithms as well as a perturbed Lagrangian formulation for contact problems. Rothert et al.[16,17] have presented a survey of techniques for contact problems with friction. They also presented a procedure involving the formulation of a boundary-value problem including friction based on an approximately known contact area and the normal stresses within this area. They presented an incremental procedure with iterations to satisfy equilibrium. All of these techniques for contact problems involve additional formulations and solution procedures. The present algorithm is attractive due to its simplicity and involves only the rearrangement of existing system matrices. No additional formulations are necessary for this procedure.

Tire Inflation and Static Contact Against Rigid Surface

The developments and procedures described previously were applied to obtain the behavior of the tire under inflation pressure and subsequent contact against a rigid surface. Some experimental results were also presented.

Tire Geometry and Finite-Element Mesh

A reference contour for the meridional profile, located as described in the section on the tire material model, is drawn to scale, and a least-squares method is used to approximate this curve in terms of tenth-degree polynomials for each of the coordinates x^1 and x^2. This, combined with the variable-order polynomial definition of geometry used in the shell formulation, provides an accurate representation of the initial profile of the tire. The geometry of the tire possesses a double symmetry and, for simplicity, a quarter of the tire is modeled using a graded mesh consisting of 108 (12 meridional $\times 9$ circumferential) finite elements. Out of this, a refined 4×4 mesh is provided in the region that is likely to be in contact. Techniques for exploiting symmetries in anisotropic structures in the context of analysis of tires have been presented by Noor et al.[18] The present mesh should be able to provide an adequate qualitative insight into the behavior of the tire. However, a more refined mesh, especially with more elements in the contact area, and modeling of the complete tire to account for nonsymmetry due to composite construction will result in more accurate predictions of footprint areas and pressure distributions. Comments on factors restricting such an extensive study at the present time are given in a later section.

Tire Inflation

The tire under investigation was inflated in increments of 5 psi up to a maximum of 45 psi. The deformed profiles of the meridian of the tire carcass for total pressures of 25 and 45 psi are shown in Fig. 1. For this analysis, the tire was assumed as fixed where it is in contact with the rim. Whereas considerable growth due to pressurization was noticed at the sidewall, the inflation did not deflect the crown considerably and acts mostly in stiffening the tire. The load-deflection curve at the sidewall is shown in Fig. 2. Plots of the deflection both normal to the tire meridian and in the horizontal direction are shown. An experimental value for the maximum section width of the tire at 35-psi inflation pressure is also shown in Fig. 2. More of such experimental data at different inflation pressures is required for a thorough validation of the numerical results.

For simplicity and convenience of presentation, all of the resulting curves for bending and twisting moments as well as membrane stress resultants for the tire with inflation but without contact are plotted on the same figures (4–10) for the case of the tire in contact with a flat rigid surface. Thus, the results for both cases, with and without contact, will subsequently be described simultaneously.

Tire Contact Against Rigid Surface

The study of the static contact of the tire against a rigid surface was done for the tire with inflation pressures of 25, 30, and 35 psi. Since the trends observed were similar in each case, only results for an inflation pressure of 35 psi are presented.

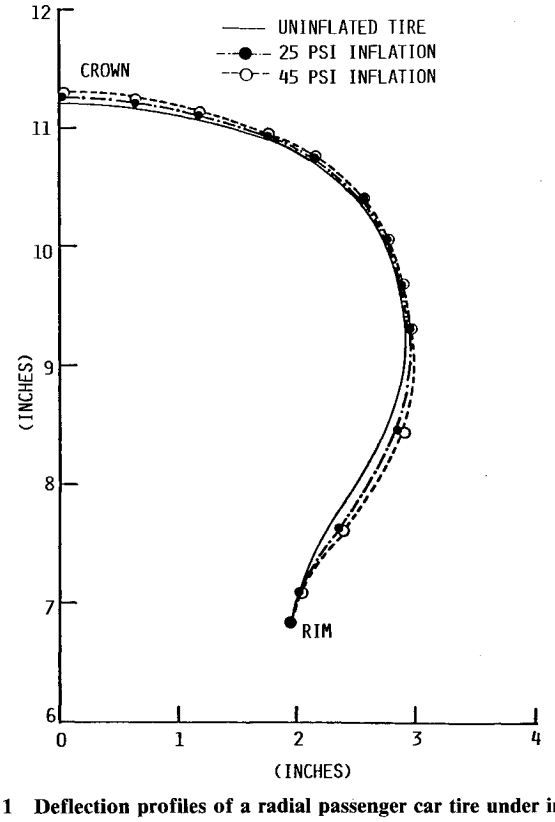

Fig. 1 Deflection profiles of a radial passenger car tire under inflation pressures.

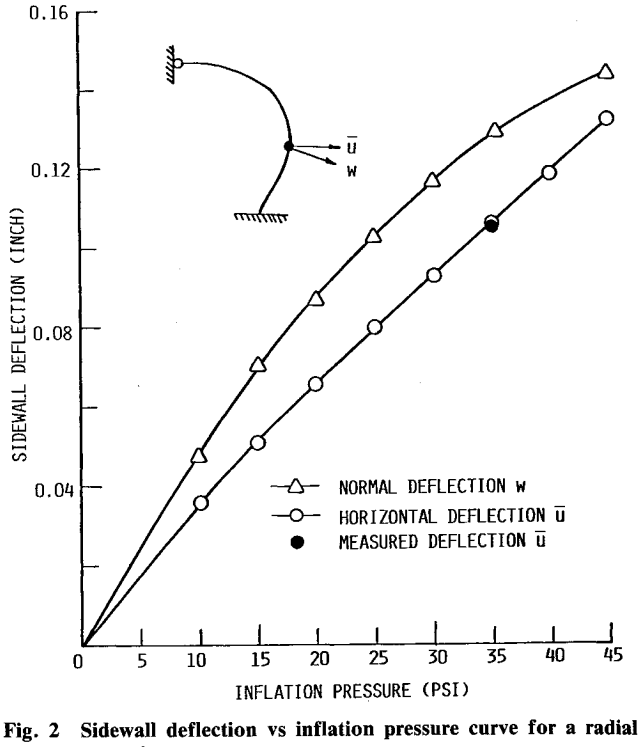

Fig. 2 Sidewall deflection vs inflation pressure curve for a radial passenger car tire.

After an initial vertical displacement of 0.2 in., the tire was given vertical displacements in increments of 0.1 in. up to a total of 0.9 in. The displacement profiles of the tire corresponding to $\phi = 0$ deg are shown in Fig. 3 for total vertical deflections of 0.3, 0.6, and 0.9 in., respectively. The solid circles in the figure represent the paths of movement of two nodal points on the sidewall for intermediate steps. The redistribution of stress and moment resultants along meridians at different circumferential locations were obtained. Some of these redistributions, corresponding to circumferential locations at $\phi = 0$, 70, and 162 deg, are shown in Figs. 4–10.

For the case of the tire with inflation but without contact, the moment and stress resultant distributions were plotted along a meridional arc of the tire carcass. The moment distributions were essentially zero, as shown by the dotted curves in Figs. 4–6, except for the meridional moment near the rim due to the presence of fixed-end boundary conditions at the rim. This suggests that the inflation of the tire is dominated by membrane action and very little bending occurs.

The meridional and circumferential stress resultant distributions under inflation pressure are shown by dotted curves in Figs. 7–10.

For the case of inflation only with no contact, the dashed curves in Figs. 7 and 8 are identical, except that the two are plotted in different scales. The two dashed curves in Figs. 9 and 10 are also identical. It is seen in Fig. 8 that meridional stress resultants are relatively small and do not vary much along the entire meridian. It is seen in Fig. 10 that the circumferential stress resultants are dominant in the region ($\xi = 0$–2 in.) reinforced by the body and belt plies. The results for the twisting stress resultant ($N_{\xi\eta}$) were practically zero everywhere, but are not shown here.

For the case of the tire in contact with $\delta = 0.9$ in., it is seen in Figs. 4–7 and 9 that considerable redistributions of moments and stress resultants occur in the region of contact (around $\phi = 0$ deg). It is also seen in Figs. 8 and 10 that, in the regions away from the contact area ($\phi = 70$ and 162 deg), the moment and stress resultants remain practically unaffected due to the contact. Of particular concern to the tire design engineer are the distributions corresponding to the resultants M_ξ (Fig. 4), $M_{\xi\eta}$ (Fig. 6), and N_η (Fig. 9).

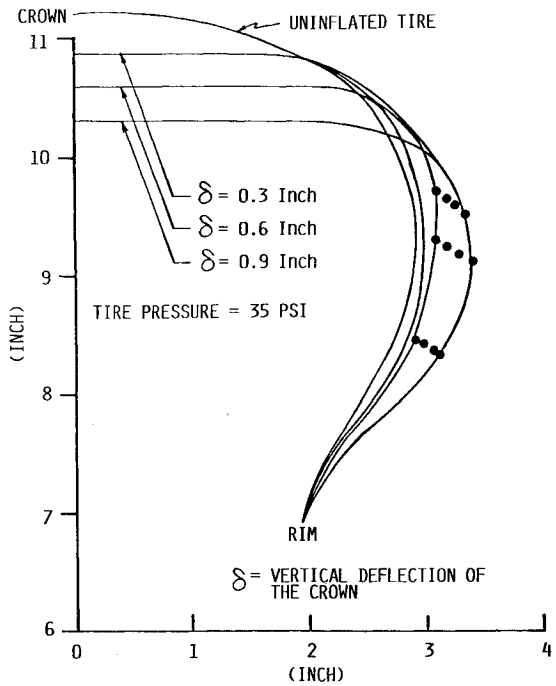

Fig. 3 Deflection profiles of the tire in contact against a rigid surface.

Figure 11 shows the footprint areas corresponding to total vertical deflections of 0.3, 0.6, and 0.9 in. of the crown with tire inflation pressure at 30 psi. Although a more refined mesh is needed for accurate prediction of the footprint, the present results seem to suggest an elliptical shape of the footprint area, which is in agreement with experimental observations. Of interest is the development of suction pressure in some area of

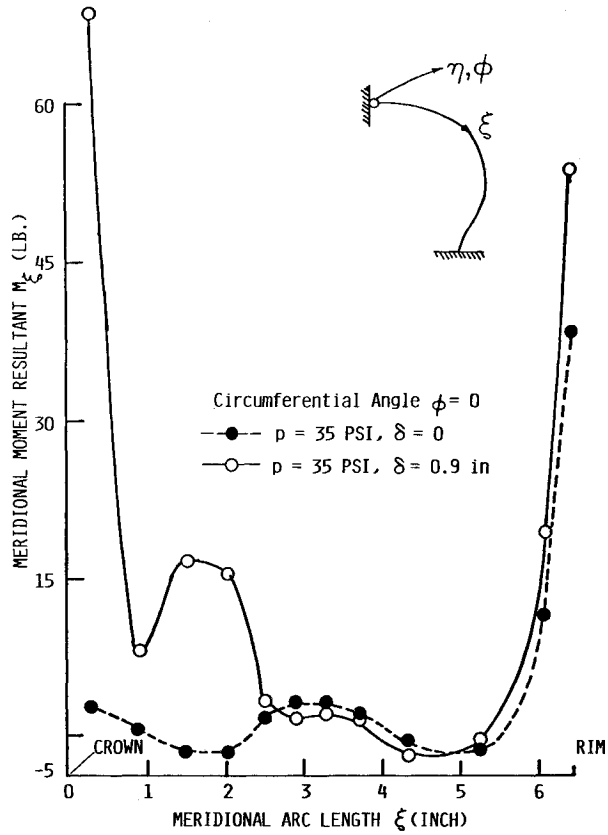

Fig. 4 Redistribution of meridional moment resultant along the meridional direction at circumferential angle $\phi = 0$ deg (p = inflation pressure, δ = vertical deflection of crown).

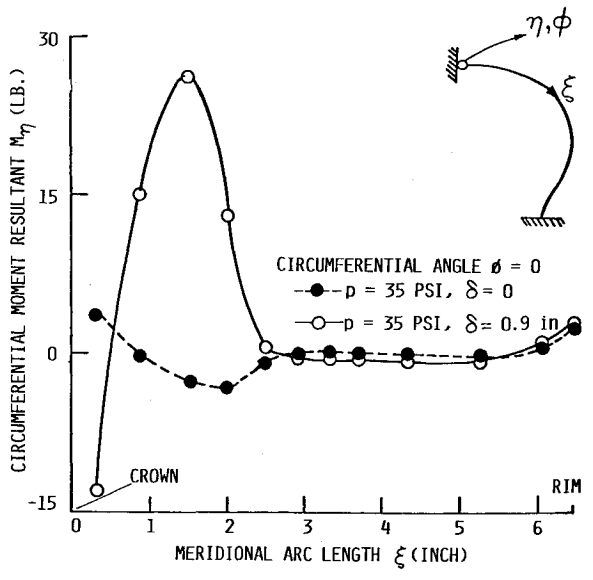

Fig. 5 Redistribution of circumferential moment resultant along meridional direction at circumferential angle $\phi = 0$ deg (p = inflation pressure, δ = vertical deflection of crown).

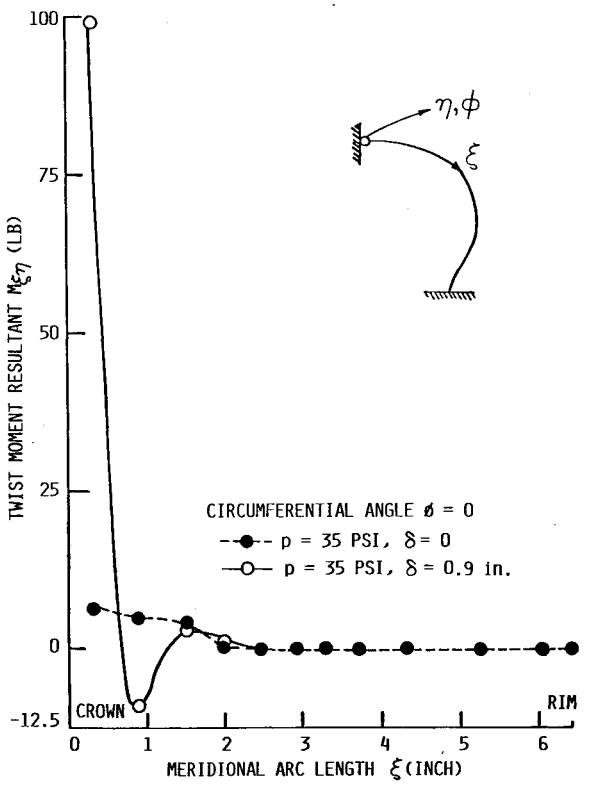

Fig. 6 Redistribution of twist moment resultant along meridional direction at circumferential angle $\phi = 0$ deg (p = inflation pressure, δ = vertical deflection of crown).

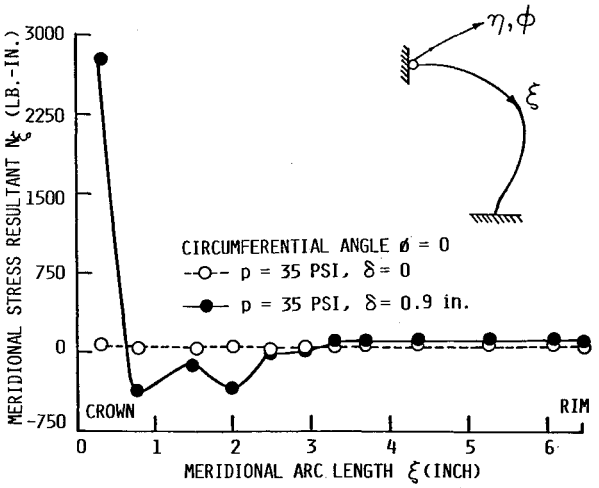

Fig. 7 Redistribution of meridional stress resultant along meridional direction at circumferential angle $\phi = 0$ deg (p = inflation pressure, δ = vertical deflection of crown).

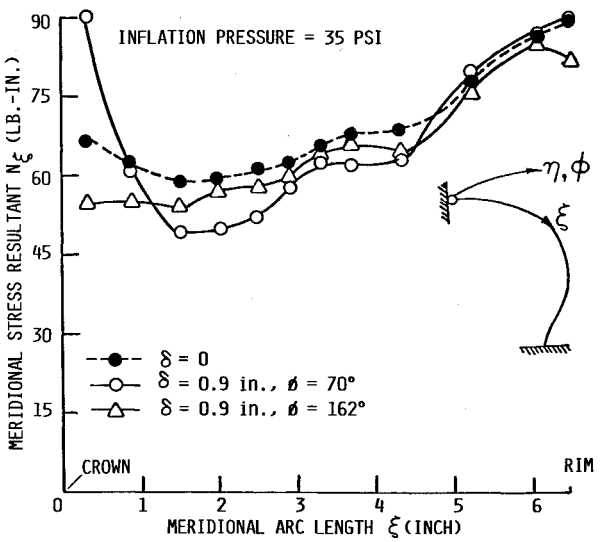

Fig. 8 Redistribution of meridional stress resultant along meridional direction for circumferential angles $\phi = 70$ and 162 deg (δ = vertical deflection of crown).

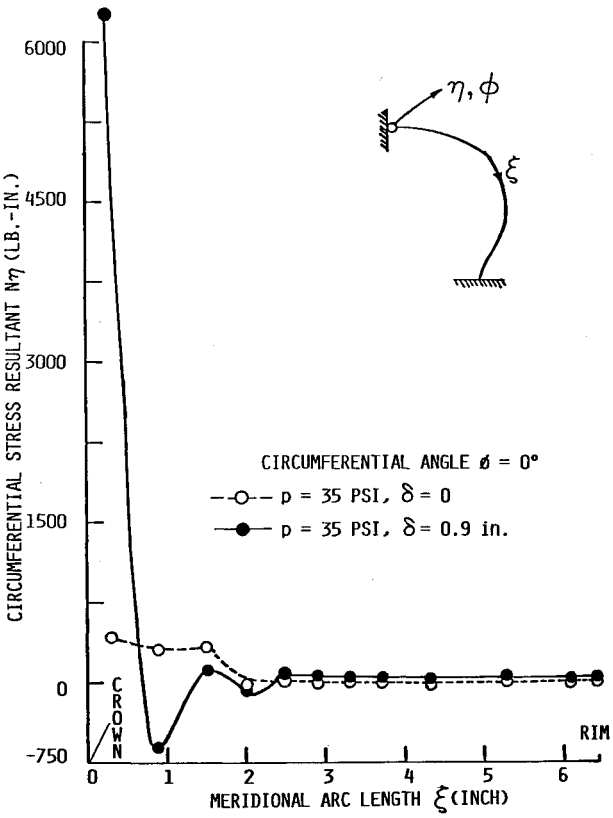

Fig. 9 Redistribution of circumferential stress resultant along meridional direction at circumferential angle $\phi = 0$ deg (p = inflation pressure, δ = vertical deflection of crown).

the footprint predicted by the present algorithm. This results because the algorithm does not provide for points inside the footprint to lift off. The tendency of contact loss in the footprint interior is not unexpected, since observations on real tires show that the load-carrying shell reference surfaces buckle inward with increasing loads. This results in a diminishment of contact pressure between tire treads and road in the interior regions of the footprint. The reason that the real footprint pressure does not become zero is that the elasticity of the compressed tire treads normal to the reference surface prevents it. In the model used here, this compressibility of the tire treads is not included, but could be added in the next step of refinement. A finer mesh with the capability of having more nodal points that may come in contact with the rigid surface and a refinement of the present algorithm may result in better predictions, as discussed in the next section. The total load required to cause the footprint deflection was obtained by summation of the nodal loads for all nodes in contact. Figure 12 shows a plot of the total vertical load applied to cause the required vertical displacement. Experimental values for the total vertical load are also shown in Fig. 12, and discrepancies between the computed and experimental results

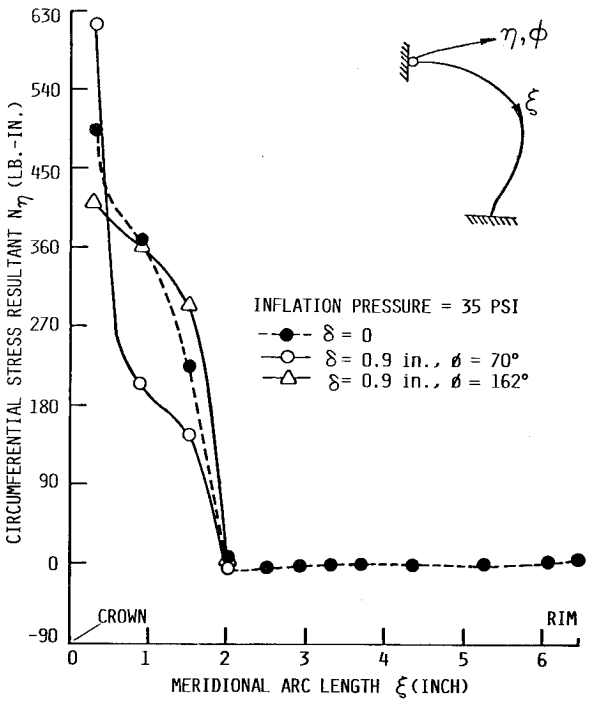

Fig. 10 Redistribution of circumferential stress resultant along meridional direction for circumferential angles $\phi = 70$ and 162 deg (δ = vertical deflection of crown).

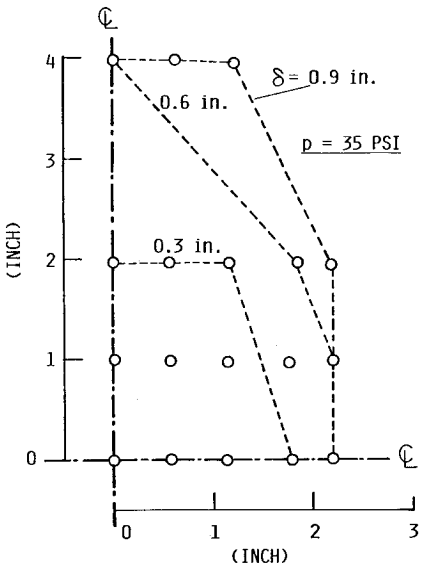

Fig. 11 Footprint areas for vertical crown deflection of 0.3, 0.6, and 0.9 in. at tire pressure of 35 psi.

were observed. Similar discrepancies were also seen in Ref. 12. A better agreement may result from refinements in formulation and solution procedure, as suggested in the next section.

Discussion and Conclusion

A finite-element procedure was applied to predict the behavior of a tire under inflation and subsequent contact against a rigid surface. A geometrically nonlinear, 48 dof, doubly curved, thin-shell finite element incorporating laminated composite material stress-strain law was employed. A load increment procedure was used for the inflation analysis, and a displacement increment procedure was used for the contact analysis. For both incremental procedures, Newton-Raphson iterations were performed to assure equilibrium of the tire.

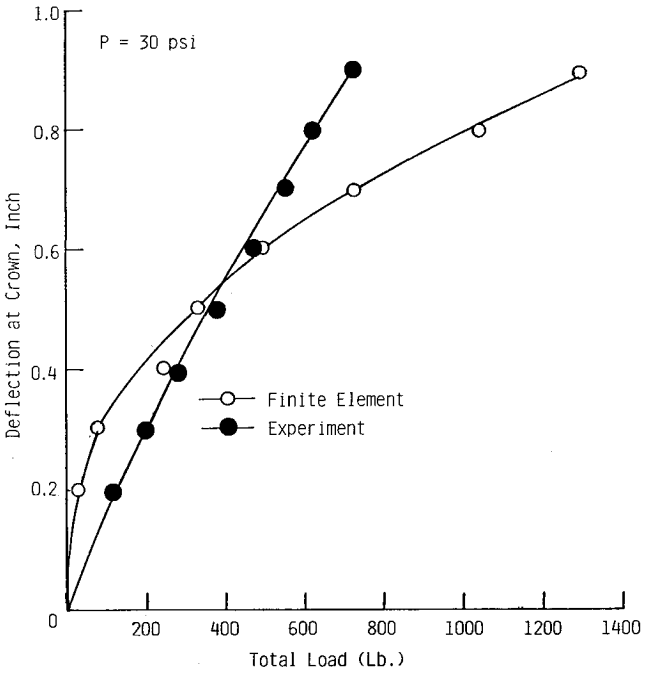

Fig. 12 Load vs deflection for contact at 30-psi pressure.

This study provided a reasonable estimate of tire deflections and stresses under inflation and subsequent static contact. The inflation of the tire resulted predominantly in membrane action. Bending occurs mostly during contact of the tire with significant effects largely in the area of contact. Qualitative trends for footprint shapes, areas, and total loads for causing a given vertical deflection were obtained. The primary limitation of the present development in this regard arises from the fact that negative (suction) reactions are allowed to develop at nodal points in contact with the rigid surface. This procedure may be refined by repeating a displacement increment step for cases when negative reactions occur at nodal points in contact and by not prescribing vertical displacement at such points. Such a refinement would, however, be meaningful only if a large number of nodes are provided in the zone likely to be in contact and the tire is pressed in very small displacement increment steps. Due to the nonlinear nature of the problem, such an effort may result in heavy computer time and costs. However, more realistic modeling of the tire, taking into account the transverse compression and elasticity of tire treads, may eliminate the need for such refinements.

Acknowledgment

This research was supported by the Firestone Tire & Rubber Company, which also provided the experimental data.

References

[1]Patel, H. P., Turner, J. L., and Walter, J. D., "Radial Tire Cord-Rubber Composites," *Rubber Chemistry and Technology*, Vol. 49, 1976, pp. 1095-1110.

[2]Patel, H. P. and Zorowski, C. F., "Deformation of the Pneumatic Tire," *Tire Science and Technology*, Vol. 6, 1978, pp. 233-247.

[3]Patel, H. P. and Kennedy, R. H., "Nonlinear Finite Element Analysis for Composite Structures of Axisymmetric Geometry and Loading," *Computers and Structures*, Vol. 15, 1982, pp. 79-84.

[4]Kennedy, R. H., Patel, H. P., and McMinn, M. S., "Radial Truck Tire Inflation Analysis: Theory and Experiment," *Rubber Chemistry and Technology*, Vol. 54, 1981, pp. 751-766.

[5]Deak, A. L., "Stress Analysis of Aircraft Tires—Vol. I: Analytical Formulation," AFFDL-TR-76-11, 1976.

[6]DeEskinazi, J., "A Finite Element Model for the Stress Analysis of Pneumatic Tires in Contact with a Flat Surface," Ph.D. thesis, Purdue University, West Lafayette, IN, May 1976.

[7]DeEskinazi, J., Yang, T. Y., and Soedel, W., "Displacement and Stresses Resulting from Contact of a Steel Belted Radial Tire with a Flat Surface," *Tire Science and Technology*, Vol. 6, 1978, pp. 48–70.

[8]Yang, T. Y. and Saigal, S., "A Curved Quadrilateral Element for Static Analysis of Shells with Geometric and Material Nonlinearities," *International Journal for Numerical Methods in Engineering*, Vol. 21, 1985, pp. 617–635.

[9]Saigal, S., Kapania, R. K., and Yang, T. Y., "Geometrically Nonlinear Finite Element Analysis of Imperfect Laminated Shells," *Journal of Composite Materials*, Vol. 20, 1986, pp. 197–214.

[10]Walter, J. D., Avgeropoulos, G. N., Janssen, M. L., and Potts, G. R., "Advances in Tire Composite Theory," *Tire Science and Technology*, Vol. 1, 1973, pp. 210–250.

[11]Bathe, K-J., *Finite Element Procedures in Engineering Analysis*, Prentice-Hall, NJ, 1982.

[12]Tielking, J. T., "Contact Solution Algorithms," Workshop on Computational Methods for Structural Mechanics and Dynamics, NASA Langley Research Center, June 1985.

[13]Oden, J. T., "Exterior Penalty Methods for Contact Problems in Elasticity," *Nonlinear Finite Element Analysis in Structural Mechanics*, edited by K-J. Bathe, E. Stein, and W. Wunderlich, Springer, Berlin, 1980.

[14]Kikuchi, N. and Oden, J.T., "Contact Problems in Elastostatics," *Special Problems in Solid Mechanics*, Vol. IV, edited by J. T. Oden and G. F. Carey, Prentice-Hall, NJ, 1984.

[15]Simo, J. C., Wriggers, P., and Taylor, R. L., "A Perturbed Lagrangian Formulation for the Finite Element Solution of Contact Problems," *Computer Methods in Applied Mechanics and Engineering*, Vol. 50, 1985, pp. 163–180.

[16]Rothert, H., Idelberger, H., Jacobi, W., and Niemann, L., "On Geometrically Nonlinear Contact Problems with Friction," *Computer Methods in Applied Mechanics and Engineering*, Vol. 51, 1985, pp. 139–155.

[17]Rothert, H., Idelberger, H., Jacobi, W., and Laging, G., "On the Finite Element Technique of the Three-Dimensional Tire Contact Problem," *Nuclear Engineering and Design*, Vol. 78, 1984, pp. 363–375.

[18]Noor, A. K., Anderson, C. M., and Tanner, J. A., "Exploiting Symmetries in the Modeling and Analysis of Tires," Workshop on Computational Methods for Structural Mechanics and Dynamics, NASA Langley Research Center, June 1985.